Nonlinear denoising of functional magnetic resonance imaging time series with wavelets

Sven Stausberg[1,2,3,*] and Klaus Lehnertz[1,3,4,†]

[1]*Department of Epileptology, Neurophysics Group, University of Bonn, Sigmund-Freud-Str. 25, 53105 Bonn, Germany*

[2]*Department of NeuroCognition, LIFE & BRAIN GmbH, Sigmund-Freud-Str. 25, 53127 Bonn, Germany*

[3]*Helmholtz-Institute for Radiation and Nuclear Physics, University of Bonn, Nussallee 14-16, 53115 Bonn, Germany*

[4]*Interdisciplinary Center for Complex Systems, University of Bonn, Römerstr. 164, 53117 Bonn, Germany*

(Received 28 February 2008; published 15 April 2009)

In functional magnetic resonance imaging (fMRI) the blood oxygenation level dependent (BOLD) effect is used to identify and delineate neuronal activity. The sensitivity of a fMRI-based detection of neuronal activation, however, strongly depends on the relative levels of signal and noise in the time series data, and a large number of different artifact and noise sources interfere with the weak signal changes of the BOLD response. Thus, noise reduction is important to allow an accurate estimation of single activation-related BOLD signals across brain regions. Techniques employed so far include filtering in the time or frequency domain which, however, does not take into account possible nonlinearities of the BOLD response. We here evaluate a previously proposed method for nonlinear denoising of short and transient signals, which combines the wavelet transform with techniques from nonlinear time series analysis. We adopt the method to the problem at hand and show that successful noise reduction and, more importantly, preservation of the shape of individual BOLD signals can be achieved even in the presence of in-band noise.

DOI: 10.1103/PhysRevE.79.041914 PACS number(s): 87.61.Qr, 05.45.Tp, 87.19.lf

I. INTRODUCTION

Investigation of neuronal activity by functional magnetic resonance imaging (fMRI) has grown to a widely used method in brain research [1]. A tight relation exists between neuronal activation, cerebral energy metabolism, and cerebral vasculature and is called the neurovascular coupling [2]. With neuronal activity the regional cerebral blood flow is increasing, which causes a change in the oxygenated to deoxygenated blood ratio. This change in blood oxygenation induces signal intensity changes in $T2^*$ weighted MRI images and is called the blood oxygenation level dependent (BOLD) effect [3].

The accurate estimation of single activation-related BOLD signals across brain regions is of particular relevance to improve understanding of the neuronal basis of hemodynamic responses. In the analysis of time-resolved fMRI data one is faced with the problem that BOLD signals typically constitute only a small fraction of the available fMRI time series and are of low amplitude. Moreover, fMRI time series are superimposed by many sources of noise and artifacts, which renders a straightforward detection of single BOLD signals by visual inspection almost impossible. In order to improve the very low signal-to-noise ratio (SNR) averaging of fMRI time series evoked by multiple repetitions of the same stimulus is commonly used. With this approach it is assumed that the repetitions lead to the same neuronal activation and BOLD signal characteristics [4]. These assumptions, however, may be inaccurate in practice and any alterations of the BOLD signal, which is known to exhibit a substantial variability [5], will lead to a destruction of signal-related components.

A method for nonlinear denoising of short and transient signals has been proposed by Effern *et al.* [6]. It combines the wavelet transform with techniques already developed for the paradigm of deterministic chaotic systems using time-delay embeddings of signals for state space reconstruction and denoising [7–9]. These techniques were shown to allow reduction of noise in a variety of physiologic data such as speech [10–12] and heart signals [13–16]. With circular state space embedding nonlinear denoising with wavelets enabled the study of individual short-lasting event-related activity against strong ongoing brain electrical activity [6,17].

Nonlinear denoising with wavelets is quite different from conventional low- or band-pass filtering in the Fourier domain, because denoising takes part in all frequency bands. Nonlinear denoising may also be better suited for the treatment of noisy fMRI time series particularly with respect to the possibly nonlinear structure of the BOLD signal [18] with which filter techniques that preferentially focus on spectral or linear properties of fMRI time series [19–27] may interact unfavorably.

We here exploit the merit of the denoising method proposed in Ref. [6] for the detection of individual BOLD signals in short and noisy fMRI time series. Since BOLD signals consist of only a limited amount of data points (typically a few ten) we do not use circular state space embedding to achieve a sufficient filling of the state space. Instead we pursue another though closely related strategy and take advantage of fMRI data acquisition which allows a dense spatial sampling (typically a few mm^3) of an activated brain region. By embedding time series from several nearby voxels, together with the one we want to denoise, and with appropriately chosen parameters of the denoising technique we show that successful noise reduction and, more importantly, preservation of the shape of individual BOLD signals in test fMRI time series can be achieved even in the presence of in-band noise.

*sven.stausberg@uni-bonn.de

†klaus.lehnertz@ukb.uni-bonn.de

This paper is organized as follows. In Sec. II we briefly recall the nonlinear denoising method proposed in Ref. [6] together with our technical implementation details. In Sec. III A we describe the results obtained from denoising test fMRI time series contaminated with white and in-band noise. Section III B is dedicated to the nonlinear denoising of experimental fMRI data sets and in Sec. IV we present our conclusions.

II. METHODS

A. Nonlinear denoising with wavelets

We assume a measured time series $y_n, n=1,\ldots,N$ to represent a superposition of the *true* signal x_n (which we want to identify) and random noise ϵ_n, i.e., $y_n=x_n+\epsilon_n$. If y_n is purely deterministic, it is restricted to a low-dimensional subspace. For the fMRI time series we are concerned with here, we assume this still to be valid. We hope to identify this direction and to correct y_n by simply projecting it onto the subspace spanned by the clean data [7,13].

In order to realize projections onto noise-free subspaces, it was proposed in Ref. [6] to calculate wavelet transforms of delay vectors and to determine signal-related components by estimating variances separately for each state space direction (see Ref. [6] for advantages of this approach over the commonly used singular value decomposition for the treatment of transient signals). With this denoising scheme, the observed time series $Y=(y_1,y_2,\ldots,y_N)$ is time-delay embedded into an m-dimensional state space, which leads to state space vectors $\boldsymbol{y}_n=(y_n,\ldots,y_{n-(m-1)\tau})$, where τ is an appropriate time delay. Next, we select a state space vector $\boldsymbol{y}_n$ we want to correct and identify its k nearest neighbors $\boldsymbol{y}_{r_{n,j}}$ using the Euclidean norm ($r_{n,j}$ with $j=0,\ldots,k$ denote the indices of the k nearest neighbors of $\boldsymbol{y}_n$, and for $\boldsymbol{y}_n$ itself, i.e., $j=0$, and $r_{n,0}=n$). We then compute the discrete wavelet transform [28] of $\boldsymbol{y}_{r_{n,j}}$ and denote the wavelet transformed state space vectors by $\boldsymbol{w}_{r_{n,j}}$. As already mentioned above, the important assumption is that the clean signal lies within a subspace of dimension $d \ll m$. Furthermore, we assume that this subspace is spanned by only a few basis functions in the wavelet domain. Now, let $C_q^{(k)}(\boldsymbol{w}_{r_n})=\langle \boldsymbol{w}_{r_{n,j}} \rangle_q$ denote the qth component of the center of mass of $\boldsymbol{w}_{r_n}$ and $\sigma_{n,q}^2$ the corresponding variance. In the case of signal-related neighbors the ratio $C_q^{(k)}(\boldsymbol{w}_{r_n})/\sigma_{n,q}^2$ is expected to be higher in signal than in noise-related state space directions, which allows one to discriminate between noisy and noise-free components in state space. Using the shrinking condition [29]

$$\tilde{w}_{n,q}=\begin{cases} w_{n,q}, & |C_q^{(k)}(\boldsymbol{w}_{r_n})| \geq 2\lambda \dfrac{\sigma_{n,q}}{\sqrt{k+1}} \\ 0, & \text{else} \end{cases} \tag{1}$$

where the threshold parameter λ and the number of nearest neighbors k depend on specific qualities of signal and noise, we project onto the noise-free subspace. From the inverse wavelet transform of $\tilde{\boldsymbol{w}}_n$ we obtain a corrected state space vector, and by applying this scheme to all remaining state space vectors the clean time series can be reconstructed.

When denoising fMRI time series one is faced with the problem that these time series typically consist of a limited amount of data points ($100<N<700$), and a proper reconstruction of the state space and detection of signal-related state space directions cannot be guaranteed. If such short-lasting time series, however, are measured repeatedly during an experiment (e.g., following a sequence of well defined stimuli) a sufficient number of delay vectors can be achieved via *circular embeddings* even for high embedding dimensions (cf. [6,17]). Nevertheless, since we here aim at denoising fMRI time series following a single stimulus only, we pursue another strategy. Given a sufficiently dense spatial sampling of an activated brain region, fMRI time series from nearby voxels exhibit a quite similar temporal evolution, apart from amplitude alterations and/or temporal jitter. We therefore expect that an embedding of fMRI time series from several nearby voxels, together with the one we want to denoise, leads to a filling of the state space, so that a sufficient number of nearest neighbors can be found for each vector. Before embedding, we normalize each fMRI time series to zero mean and unit variance.

In order to allow an accurate signal reconstruction in state space the parameters embedding dimension m, time delay τ, thresholding coefficient λ, as well as the number of nearest neighbors k have to be chosen appropriately. Several methods have been developed to estimate "optimal" parameters depending on specific aspects of the given data (e.g., noise level, type of noise, stationarity, etc.) [7]. These methods, however, assume that the clean signal is indeed low dimensional, an assumption we are not ready to make in the case of fMRI time series. Thus, we approached the problem of "optimal" parameters empirically. Parameters τ and m are not independent from each other. In particular, high embedding dimensions allow small time delays and vice versa. We here estimated "optimal" embedding dimensions, thresholding coefficients, and number of neighbors by varying m, λ, and k for a fixed $\tau=1$ and a fixed number of nearby (in the nearest-neighbor sense) voxels $L=6$. To allow fast wavelet transform, we chose m to be a power of 2. We here use a Daubechies mother wavelet of order 4 [30]. In preliminary investigations we tested Daubechies wavelets up to the order of 20 as well as different wavelet basis function and observed that both had a negligible influence on the denoising performance (cf. [26]).

B. Generating noisy test fMRI time series

We simulated a so-called four-dimensional (4D) fMRI volume, which consisted of N sequentially acquired three-dimensional (3D) volumes with $64\times64\times30$ voxels each. N is thus the total number of data points of a fMRI time series in a given voxel ν and is composed of intensity values I sampled at discrete times $t_n=n\Delta t, n=1,\ldots,N, T=N\Delta t$, where Δt denotes a properly chosen sampling interval. For a fixed observation time T and for some voxel ν we generated a noisy fMRI time series

$$I_n^{(\nu)}=O^{(\nu)}+I_n^B+\epsilon_n^{(\nu)}, \tag{2}$$

where $O^{(\nu)}$ denotes a constant intensity offset and $\epsilon_n^{(\nu)}$ represents the noise contribution. The BOLD signal I_n^B is de-

rived from a convolution of the hemodynamic response function [31]

$$f_n = \sum_{i=1}^{3} (-1)^i \frac{l_i^{h_i} (t_n \kappa)^{(h_i-1)} e^{-l_i(t_n\kappa)}}{\Gamma(h_i)} \quad (3)$$

with some stimulus function (we here used a Dirac-type stimulus function that was switched on at $n_{\mathrm{on}} \equiv n = 99$). We used the Gamma function $\Gamma(x)$, respectively, its probability density function [32], to simulate the initial dip [33,34], and the positive over- and negative undershoot. For the scale parameters we used $l_1 = l_2 = l_3 = 0.2$ and set the form parameters to $h_1 = 16$, $h_2 = 6$, and $h_3 = 2$. The parameter κ was set to 4.4. Note that with these parameter settings our test fMRI time series—consisting of $N \in \{128, 256, 512\}$ data points—contained relevant components of the BOLD signal that extended over $n_{\mathrm{BOLD}} \in \{5, 10, 20\}$ data points only.

Before adding noise we rescaled the BOLD signal I_n^B such that the relative signal change $\Delta I^{(\nu)} = \frac{I_{\max}^B - O^{(\nu)}}{O^{(\nu)}}$ amounted to 1% in all simulations ($I_{\max}^B$ denotes the peak amplitude of the simulated BOLD signal). We controlled the strength of the noise contamination $\epsilon_n^{(\nu)}$ by the signal-to-noise ratio (SNR), which we here define as $R = \sigma_B^2 / \sigma_N^2$, where σ_B^2 denotes the variance of the rescaled BOLD signal and σ_N^2 the variance of the noise. We used Gaussian white noise with zero mean or a superposition of white and in-band noise [24,35]. The latter was generated by adding low-amplitude ($R = 0.1$) white noise to a phase randomized surrogate [36] of the BOLD signal, which approximately retains the power spectrum of the noise-free BOLD signal. In the following, we refer to this type of noise as in-band noise.

Intensity offset values $O^{(\nu)}$ were taken from a set of experimentally derived 4D fMRI volumes (five volunteers participating in different fMRI experiments that were acquired with two different MR scanners (1.5 and 3 T) from the same manufacturer). Randomly selected 3D volumes from this set served as templates for our simulations and the known distribution of their intensity offset values allowed us to properly place voxels of interest into the brain volume.

For the generation of noisy activation patterns we used different 3D spatial activation functions (a Gaussian function with j voxels at full width at half maximum in each direction, a triangular as well as a boxcar function with j voxels base length in each direction). We randomly selected a reference voxel ν^{ref} (in the brain volume) and—given the properties of a chosen activation function—assigned fMRI time series to voxel ν^{ref} and its nearby voxels using the methods described above. Note that this procedure—except for the boxcar activation function—lowered the SNR in each nearby voxel in dependence on its distance to the reference voxel.

C. Measuring denoising efficiency

Appropriate choice of parameters, in particular embedding dimension m, thresholding coefficient λ, as well as the number of neighbors k is important for accurate signal reconstruction in state space. We here assessed the efficiency of our denoising technique using the following measures.

For the time segments before ($n \in \{1, n_{\mathrm{on}} - 1\}$) and after the BOLD signal ($n \in \{n_{\mathrm{on}} + n_{\mathrm{BOLD}} + 1, N\}$) we consider the *noise reduction factor* $\gamma = (\sigma_t^2 - \sigma_d^2)/\sigma_t^2$, where σ_d^2 denotes the variance of the denoised time series and σ_t^2 is the variance of the noisy time series. $\gamma = 1$ (i.e., $\sigma_d^2 = 0$) indicates optimal noise reduction.

With the linear correlation coefficient r we measure the *similarity* between the denoised and the noise-free BOLD signal, taking into account the time segment that includes the BOLD signal only ($n \in \{n_{\mathrm{on}}, n_{\mathrm{on}} + n_{\mathrm{BOLD}}\}$). For $r = 1$ the denoised and noise-free BOLD signal intensity values are identical and our denoising technique fully preserves the original BOLD signal shape.

III. RESULTS

A. Denoising test fMRI time series

In order to estimate "optimal" values for the embedding dimension m, thresholding coefficient λ, and number k of nearest neighbors in state space we determined γ and r for test fMRI time series contaminated with noise (white and in-band noise) of different strength ($R \in \{0.01, 0.1, 1\}$). For each 3D spatial activation function (with $j = 3$) we simulated 50 independent 4D fMRI volumes. In each volume, we randomly chose a reference voxel—located in the brain volume—together with its L nearby voxels and assigned noisy fMRI time series ($N \in \{128, 256, 512\}$) to these voxels (cf. Sec. II B). We then applied our technique to denoise the fMRI time series from the reference voxel.

In the following we present our findings for $N = 256$ and for a 3D Gaussian activation function. Using other activation functions we obtained almost identical results (within the range of errors) for "optimal" denoising parameters. In order to cover relevant components of the BOLD signal ($n_{\mathrm{BOLD}} = 5$ for $N = 128$; cf. Sec. II B) we followed Ref. [6] and used $m = 4$ as minimum embedding dimension. The highest embedding dimension was bounded by the number of data points N, thus allowing $m = 256$.

In Fig. 1 we show for $R \in \{0.01, 0.1, 1\}$ the dependence of r and γ on the number k of nearest neighbors and on the embedding dimension m. We were able to identify a range of k values for which r remained almost constant [$r(R = 0.01) = 0.41 \pm 0.04$, $r(R = 0.1) = 0.85 \pm 0.02$, and $r(R = 1) = 0.96 \pm 0.08$]. This range had an upper bound near the maximum number $k_{\max} = [N - (m-1)\tau](L+1) - 1$ of available state space vectors. Within this range r attained significant values ($p < 0.05; r \geq 0.52$) but for $R \in \{0.1, 1\}$ only.

For all investigated SNR γ attained highest values (i.e., $\gamma \to 1$) for k close to $k_{\max}$, but in this range we already observed $r \to 0$, indexing a complete destruction of the BOLD signal. This is in line with theoretical considerations indicating that signal detection in state space is not possible when selecting k too high. Only an embedding dimension $m = 128$ allowed lower values of k, where both γ and r attained high values. Detailed investigations for $k \in [1, 50]$, $\lambda = 1$, and $m = 128$ (see left panel of Fig. 2) revealed that $k \approx 10$ led to a successful noise reduction [$\gamma(R = 0.01) = 0.83 \pm 0.02$, $\gamma(R = 0.1) = 0.85 \pm 0.02$, and $\gamma(R = 1) = 0.96 \pm 0.02$] and high values of r, at least for $R \in \{0.1, 1\}$ [$r(R = 0.01) = 0.43 \pm 0.12$, $r(R = 0.1) = 0.88 \pm 0.01$, and $r(R = 1) = 0.98 \pm 0.01$]. Selecting

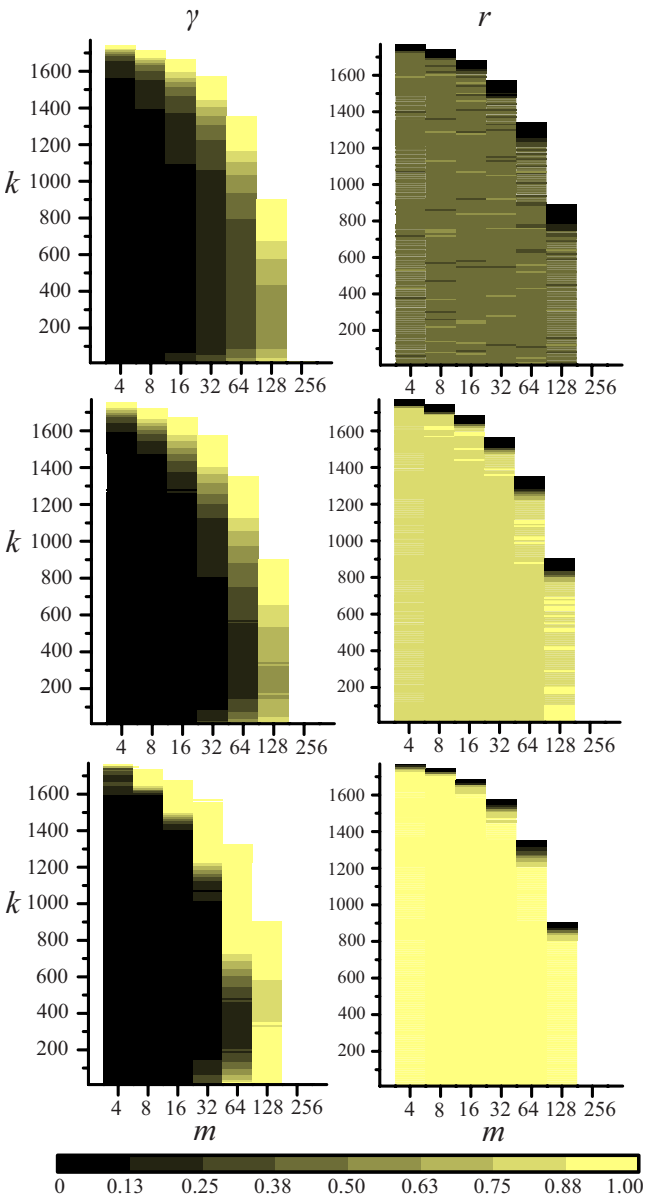

FIG. 1. (Color online) Dependence of the noise reduction factor γ (left) and the similarity measure r (right) on the number k of nearest neighbors and on the embedding dimension m for different SNR (top: $R=0.01$; middle: $R=0.1$; bottom: $R=1$) and $\lambda=1$. The mean values of γ and r are plotted for $k \leq k_{\max}$. 50 test fMRI time series superimposed with white noise ($N=256$; $n_{\mathrm{BOLD}}=10$).

lower values of k ($k<10$) resulted in higher values for γ but also in slightly lower values for r for all SNR. From these findings and from the corresponding studies using in-band noise (cf. Tables I and II) we conclude that the choice of $k=10$ and $m=128$ can be regarded as "optimal" for time series that consist of $N=256$ data points. Investigations for $N \in \{128,512\}$ necessitated an adjustment of the embedding dimension ($m=64$ for $N=128$, $m=256$ for $N=512$) but the "optimal" value of nearest neighbors remained at $k=10$. We obtained qualitatively similar results for other values of λ within the range $[0.1, 2.0]$.

In the right panel of Fig. 2 we show the dependence of γ and r on the thresholding coefficient λ. Using "optimal" values for k and m we identified for $R \in \{0.1,1\}$ a range of values $\lambda \in [1.0,1.5]$ for which both efficiency measures attained maximum values ($R=1$: $0.97<r<0.99$, $0.95<\gamma<0.99$; $R=0.1$: $0.55<r<0.96$, $0.82<\gamma<0.99$). For $R=0.01$ r attained nonsignificant mean values only ($r=0.52$ for $p<0.05$) and decreased rapidly for $\lambda>1.5$. Taking into account the characteristics of r and γ, however, choosing λ

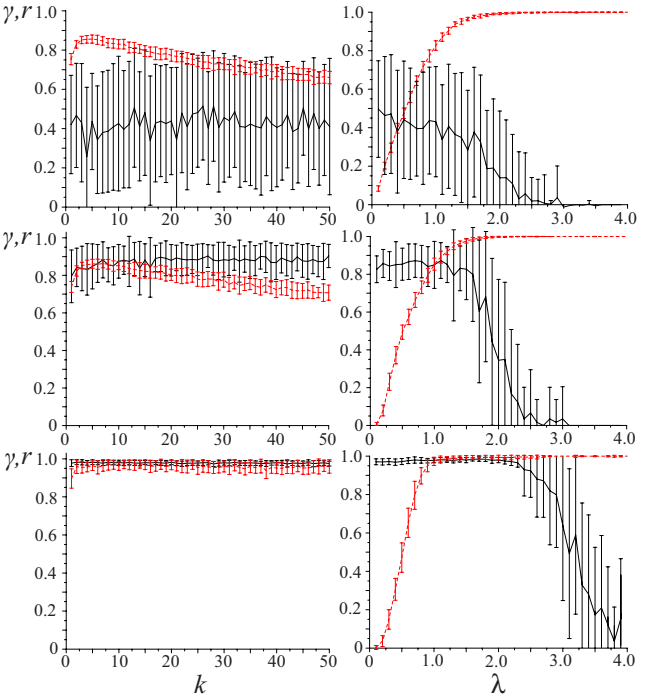

FIG. 2. (Color online) Dependence of the noise reduction factor γ (red, dotted line) and the similarity measure r (black, straight line) on the number of k nearest neighbors (left, $\lambda=1$) and on the thresholding coefficient λ (right, $k=10$) for different SNR (top: $R=0.01$; middle: $R=0.1$; bottom: $R=1$) and $m=128$. Error bars denote standard deviations derived from 50 test fMRI time series superimposed with white noise ($N=256$; $n_{\mathrm{BOLD}}=10$).

TABLE I. Summary of results obtained from denoising 50 test fMRI time series consisting of N data points and contaminated with white noise at different SNR using "optimal" parameters. Means and standard deviations of similarity measure r and the noise reduction factor γ.

$N=128$	$R=0.01$	$R=0.1$	$R=1$
r	0.35 ± 0.47	0.85 ± 0.03	0.98 ± 0.02
γ	0.72 ± 0.04	0.74 ± 0.05	0.95 ± 0.04
$N=256$	$R=0.01$	$R=0.1$	$R=1$
r	0.43 ± 0.34	0.88 ± 0.09	0.98 ± 0.01
γ	0.83 ± 0.02	0.85 ± 0.02	0.96 ± 0.02
$N=512$	$R=0.01$	$R=0.1$	$R=1$
r	0.43 ± 0.20	0.92 ± 0.05	0.98 ± 0.01
γ	0.89 ± 0.01	0.92 ± 0.02	0.99 ± 0.01

TABLE II. Same as Table I but for contaminations with in-band noise.

$N=128$	$R=0.01$	$R=0.1$	$R=1$
r	0.40 ± 0.59	0.82 ± 0.20	0.98 ± 0.02
γ	0.65 ± 0.05	0.66 ± 0.06	0.92 ± 0.07
$N=256$	$R=0.01$	$R=0.1$	$R=1$
r	0.39 ± 0.42	0.81 ± 0.15	0.98 ± 0.01
γ	0.63 ± 0.04	0.61 ± 0.04	0.93 ± 0.05
$N=512$	$R=0.01$	$R=0.1$	$R=1$
r	0.38 ± 0.42	0.82 ± 0.15	0.98 ± 0.01
γ	0.44 ± 0.03	0.44 ± 0.04	0.68 ± 0.08

$\in [0.5, 1.0]$ might be more appropriate to achieve a sufficient noise reduction without additionally lowering r. Again we observed similar dependencies for contaminations with in-band noise (cf. Table II) and thus conclude $\lambda=1$ as an applicable parameter. We obtained qualitatively similar results for time series consisting of $N=128$ and $N=512$ data points.

Exemplary test fMRI time series contaminated with white and in-band noise along with the denoised time series are shown in Fig. 3. In Tables I and II we summarize our results obtained from denoising time series with different number of data points, contaminated with white and in-band noise at different SNR, and using "optimal" parameters. Our denoising technique allowed a good noise reduction and preserved significantly the BOLD signal shape for $R \in \{0.1, 1\}$. As expected we obtained a declined performance for contaminations with in-band noise.

Before closing this section, we briefly discuss two special cases that occur when denoising a complete 4D volume data set. First, if the reference voxel is located on the boundary of the brain volume, there may be steep spatial intensity gradients within the L voxels. Since the normalization (zero mean and unit variance) of the time series before state space embedding compensates for strong intensity transitions, denoising efficiency should not be affected. Second, if the reference voxel is located on the boundary of a rectangular volume data set, the number of nearby voxels time series is reduced ($L<6$), leading to a worse representation of signal-related directions in state space. In typical fMRI volume data sets, however, voxels that are located on the boundary of a rectangular volume data set usually do not carry relevant information, and a noise reduction can be attained even with a reduced number of nearby voxels time series. In other cases, the choice of appropriate boundary conditions may help to increase L. Using the respective simulation setups we were able to confirm these theoretical predictions (results not shown here). Finally, we mention that when sequentially denoising a 4D volume data set the inclusion of already denoised time series from nearby voxels may necessitate an adjustment of parameters, particularly k and λ.

B. Denoising experimental fMRI time series

In this section we present our findings obtained from denoising experimental fMRI time series. Data set no. 1 (matrix size: 64×64, voxel size: $3 \times 3 \times 3.3$ mm^3, 35 slices) was acquired at 1.5 T from a blocked paradigm with a motor task that consisted of alternating right and left fist clenching for 21 s and 3 s rest between each hand change. With a sampling interval of $\Delta t=3$ s the fMRI time series consisted of $N=160$ data points. Data set no. 2 (matrix size: 64×64, voxel size: $3 \times 3 \times 3$ mm^3, 64 slices) is publicly available [37]. Data were acquired at 2 T from a blocked paradigm with an auditory stimulation. Rest blocks alternated with blocks of auditory stimulation (60 bisyllabic words/min presented binaurally), and each of the 16 blocks lasted for 42 s. With a sampling interval of $\Delta t=7$ s the original fMRI time series consisted of $N=96$ data points.

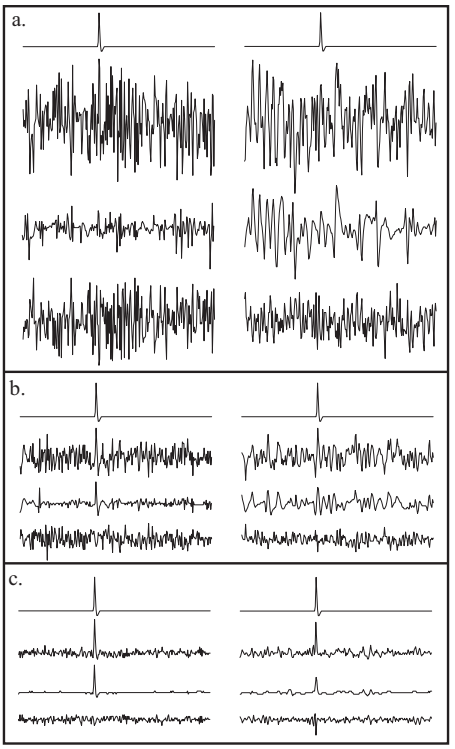

FIG. 3. Denoising test fMRI time series contaminated with different types of noise (left: white noise; right: in-band noise) at different SNR. (a) $R=0.01$, Top to bottom: BOLD signal, BOLD signal+noise, denoised signal, residual noise. (b) Same as (a) but for $R=0.1$. (c) Same as (a) but for $R=1$. The BOLD signal extents over $n_{\mathrm{BOLD}}=10$ data points ($N=256$, $n_{\mathrm{on}} \equiv n=99$, and $\Delta I^{(\nu)}=1\%$).

Before state space reconstruction we removed—by linear detrending—long-lasting drifts that are typical in experimental fMRI data [38] and, for each voxel, rescaled the time series to zero mean and unit variance. We denoised the complete 4D fMRI volumes with parameters $\lambda=1$ and $k=10$. Due to the different number of data points we used $m=128$ for data set no. 1 and $m=64$ for data set no. 2 (cf. Sec. III A). For each voxel, we calculated the linear correlation coefficient r_r between the normalized raw time series and the normalized expected BOLD signal, which we derived from convolving Eq. (3) with an experiment-specific stimulus boxcar function (data set no. 1: duration: 21 s; data set no. 2: duration: 42 s). The linear correlation coefficient r_d between the denoised time series and the normalized expected BOLD signal was calculated accordingly.

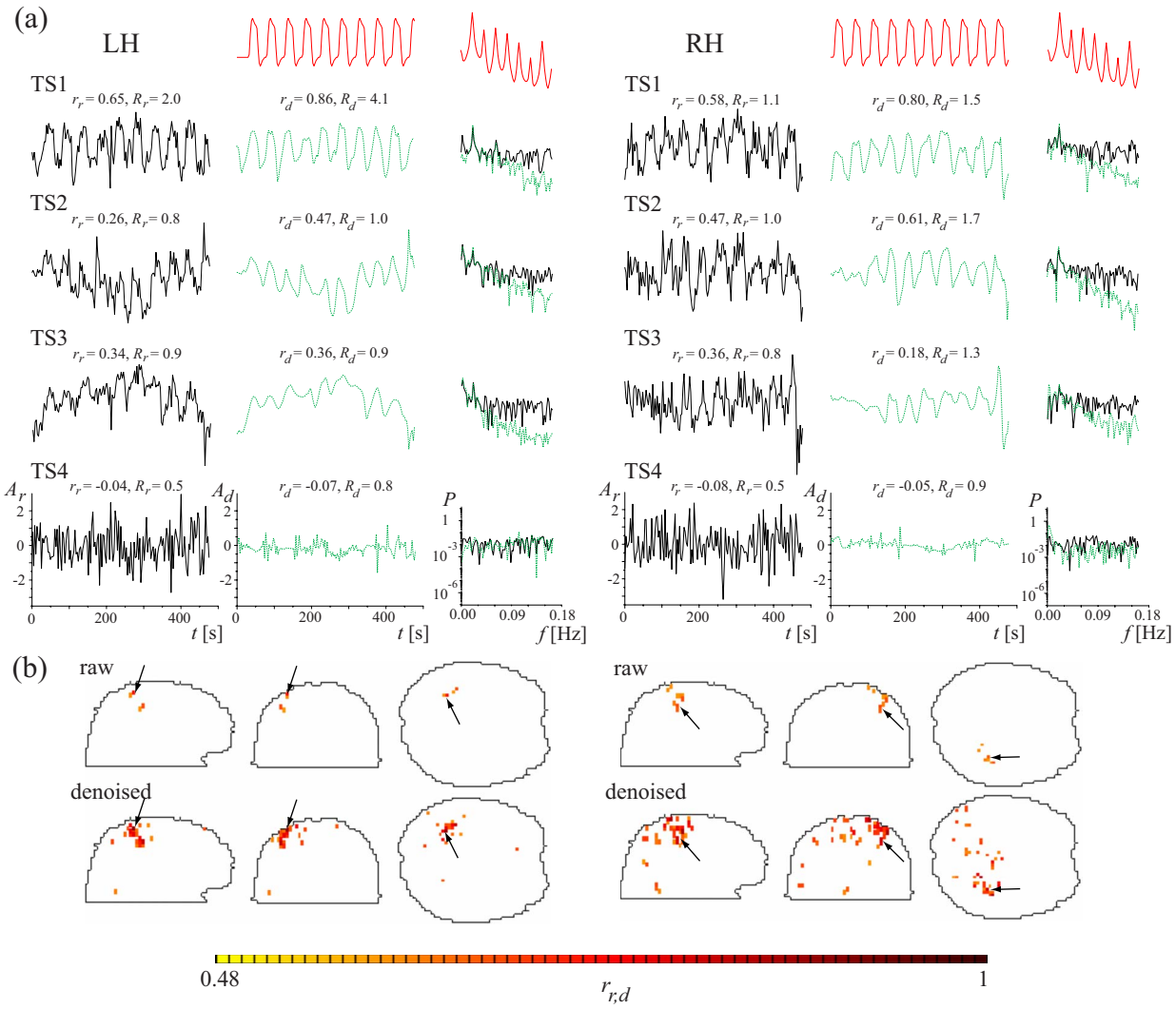

FIG. 4. (Color online) (a) Exemplary normalized raw (black, straight line) and their denoised fMRI time series (green, dotted line) from data set no. 1 together with their Fourier spectra from the left (LH) and right (RH) brain hemisphere. A_r (A_d) denotes amplitude values of the normalized raw (denoised) time series and P the power spectral density estimate. The expected BOLD signals and their Fourier spectra for each hemisphere are shown on top. Similarity between normalized raw (denoised) fMRI time series and normalized expected BOLD signals is estimated using the linear correlation coefficient r_r (r_d). For each hemisphere, fMRI time series denoted as TS1 exhibited highest similarity to the expected BOLD signal, while time series TS2–TS4 are from voxels with an increasing distance to the voxel from which TS1 was taken. R_r (R_d) denotes the estimated signal-to-noise ratio of each raw (denoised) fMRI time series. (b) Voxels at which the similarity between raw (r_r; top row) or denoised fMRI time series (r_d; bottom row) and expected BOLD signals exceeds a predefined threshold value (0.48) are shown as color-coded through projections onto orthogonal sections (left: sagittal; middle: coronal; right: axial) of the brain volume. The arrows mark the voxel from which time series TS1 was taken.

In Figs. 4(a) and 5(a) we show exemplary normalized raw and their denoised fMRI time series from data sets no. 1 and no. 2 along with the corresponding Fourier spectra [39]. Our denoising technique drastically reduced noise in all frequency bands and allowed one to detect even single BOLD responses in the fMRI time series. In order to quantify the noise reduction we estimated the signal-to-noise ratio gain $G=R_d/R_r$, where $R_d=\sigma_B^2/\sigma_{N,d}^2$ and $R_r=\sigma_B^2/\sigma_{N,r}^2$ denote the signal-to-noise ratios for the normalized raw and their denoised time series, respectively. We used the variance of the normalized expected BOLD signal as an estimate for σ_B^2. The variances of the residual time series [difference between normalized raw (respectively denoised) fMRI time series and normalized expected BOLD signal] served as estimates for $\sigma_{N,r}^2$ ($\sigma_{N,d}^2$). For the presented fMRI time series our denoising technique resulted in a signal-to-noise ratio gain of $G=1.6\pm0.3$.

In part (b) of Figs. 4 and 5 we show voxels for which the correlation coefficients r_r and r_d exceeded some predefined threshold value. The locations of these voxels coincide quite well with brain regions that had been identified as being activated in similar fMRI experiments (see, e.g., Refs. [40,41]). Due to the noise reduction, however, we observe an increased number of voxels for which their fMRI time series exhibit a higher similarity to the expected BOLD signal (cf. [24]). Whether these voxels reflect brain areas subserving specific functions should be addressed in future studies.

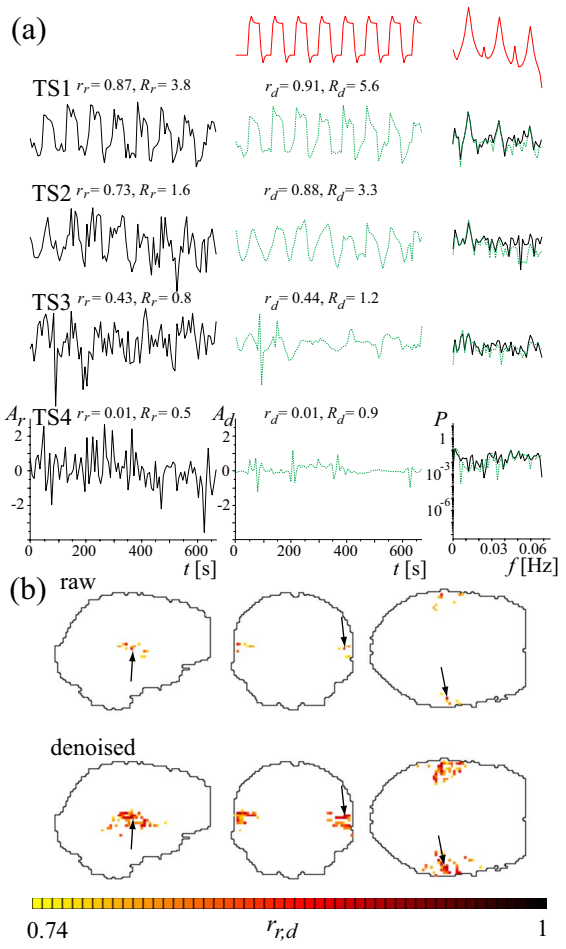

FIG. 5. (Color online) Same as Fig. 4 but for the fMRI time series from data set no. 2 and with a threshold value of 0.74.

IV. CONCLUSION

We exploited an analysis method originally proposed in Ref. [6] for the nonlinear denoising of short and transient fMRI time series. A proper time-delay embedding of signals for state space reconstruction and the detection of signal-related state space directions require a large number of data points [7,9], which is usually not available from typical fMRI time series. We therefore embedded fMRI time series from several nearby voxels, together with the one we want to denoise, assuming that an activated brain region can be spatially sampled sufficiently dense and that fMRI time series from voxels covering an activated brain region exhibit a similar temporal evolution. With appropriately chosen parameters we achieved a filling of the state space that allowed successful noise reduction and, moreover, preservation of the shape of single BOLD signals in test fMRI time series even in the presence of in-band noise.

Although our nonlinear denoising scheme requires the appropriate choice of several parameters that are important for an accurate signal reconstruction in state space, we were able to narrow down the range of possible values for some parameters and to identify optimal values for the remaining parameters. Nevertheless, it should be noted that nonlinear noise reduction is rather computationally expensive, in particular if compared to Fourier-based filters. For small and intermediate noise levels, this can be moderated by using fast neighbor search strategies [42,43]. Further improvements may also be obtained by using nonlinear noise reduction schemes that are based on reference data sets [16]. Future studies will have to reveal whether our nonlinear denoising scheme can be regarded as an alternative to other more standard noise reduction methods [19–27].

For the denoising of experimentally acquired time series we chose parameters that allowed one to preserve the shape of BOLD signals in our test fMRI time series evoked by a single Dirac-type stimulus. Although this choice may not be optimal for the experimental fMRI time series analyzed here, our denoising technique nevertheless allowed us to identify single BOLD signals from block design experiments where long duration stimulus and control blocks are repeated. Current fMRI studies use so called event-related designs [44] with several different stimuli conditions in a more random presentation. Such a design leads to a more complicated and potentially more noisy expected BOLD response, if stimuli are presented too rapidly. We expect though that the utility of our techniques for the denoising of appropriately sampled event-related fMRI time series can be demonstrated in future studies. Using our denoising technique together with data-driven, model-free analysis methods [45,46] may lead to an improved activation detection, and together with new experimental fMRI designs this may provide new insights into brain dynamics.

ACKNOWLEDGMENTS

We are grateful to Stephan Bialonski and Jens Prusseit for helpful comments on earlier versions of the paper, and to Bernd Weber and Klaus Fließbach at the Department of NeuroCognition, LIFE & BRAIN GmbH, for providing fMRI data. K.L. acknowledges support from the Deutsche Forschungsgemeinschaft.

[1] N. K. Logothetis, Nature (London) **453**, 869 (2008).
[2] C. S. Roy and C. S. Sherrington, J. Physiol. **11**, 85 (1890).
[3] S. Ogawa, T. M. Lee, A. R. Kay, and D. W. Tank, Proc. Natl. Acad. Sci. U.S.A. **87**, 9868 (1990).
[4] R. L. Buckner, P. A. Bandettini, K. M. O'Craven, R. L. S. S. E. Petersen, M. E. Raichle, and B. R. Rosen, Proc. Natl. Acad. Sci. U.S.A. **93**, 14878 (1996).
[5] G. K. Aguirre, E. Zarahn, and M. D'esposito, Neuroimage **8**, 360 (1998).
[6] A. Effern, K. Lehnertz, T. Schreiber, T. Grunwald, P. David, and C. E. Elger, Physica D **140**, 257 (2000).
[7] P. Grassberger, R. Hegger, H. Kantz, C. Schafrath, and T.

Schreiber, Chaos **3**, 127 (1993).
[8] E. J. Kostelich and T. Schreiber, Phys. Rev. E **48**, 1752 (1993).
[9] H. Kantz and T. Schreiber, *Nonlinear Time Series Analysis* (Cambridge University Press, Cambridge, UK, 2003).
[10] R. Hegger, H. Kantz, and L. Matassini, Phys. Rev. Lett. **84**, 3197 (2000).
[11] L. Matassini, H. Kantz, J. Holyst, and R. Hegger, Phys. Rev. E **65**, 021102 (2002).
[12] X. Luo, J. Zhang, and M. Small, Phys. Rev. E **72**, 046710 (2005).
[13] T. Schreiber and D. T. Kaplan, Chaos **6**, 87 (1996).
[14] T. Schreiber and D. T. Kaplan, Phys. Rev. E **53**, R4326 (1996).
[15] M. Richter, T. Schreiber, and D. T. Kaplan, IEEE Trans. Biomed. Eng. **45**, 133 (1998).
[16] K. Sternickel, A. Effern, K. Lehnertz, T. Schreiber, and P. David, Phys. Rev. E **63**, 036209 (2001).
[17] A. Effern, K. Lehnertz, G. Fernández, T. Grunwald, P. David, and C. E. Elger, Clin. Neurophysiol. **111**, 2255 (2000).
[18] A. L. Vazquez and D. C. Noll, Neuroimage **7**, 108 (1998).
[19] B. Biswal, A. E. DeYoe, and J. S. Hyde, Magn. Reson. Med. **35**, 107 (1996).
[20] F. Kruggel, D. Y. von Cramon, and X. Descombes, Neuroimage **10**, 530 (1999).
[21] K. J. Friston, O. Josephs, E. Zarahn, A. P. Holmes, S. Rouquette, and J. B. Poline, Neuroimage **12**, 196 (2000).
[22] J. Tanabe, D. Miller, J. Tregellas, R. Freedman, and F. G. Meyer, Neuroimage **15**, 902 (2002).
[23] O. Friman, M. Borga, P. Lundberg, and H. Knutsson, Neuroimage **22**, 645 (2004).
[24] J. A. de Zwart, P. van Gelderen, M. Fukunaga, and J. H. Duyn, Magn. Reson. Med. **59**, 939 (2008).
[25] M. E. Alexander, R. Baumgartner, C. Windischberger, E. Moser, and R. L. Somorjai, Magn. Reson. Imaging **18**, 1129 (2000).
[26] S. M. LaConte, S. C. Ngan, and X. Hu, Magn. Reson. Med. **44**, 746 (2000).
[27] S. C. Ngan, S. M. LaConte, and X. Hu, Neuroimage **11**, 797 (2000).
[28] C. K. Chui, *An Introduction to Wavelets* (Academic Press, San Diego, 1992).
[29] D. L. Donoho, I. M. Johnstone, and B. W. Silverman, IEEE Trans. Inf. Theory **41**, 613 (1995).
[30] I. Daubechies, *Ten Lectures on Wavelets* (Society for Industrial and Applied Mathematics, Pennsylvania, 1992).
[31] G. H. Glover, Neuroimage **9**, 416 (1999).
[32] M. Evans, N. Hastings, and B. Peacock, *Statistical Distributions* (Wiley, New York, 1993).
[33] X. Hu, T. H. Le, and K. Ugurbil, Magn. Reson. Med. **37**, 877 (1997).
[34] E. Yacoub, A. Shmuel, J. Pfeuffer, P. F. Van de Moortele, G. Adriany, K. Urgurbil, and X. Hu, NMR Biomed. **14**, 408 (2001).
[35] P. L. Purdon and R. M. Weisskoff, Hum. Brain Mapp. **6**, 239 (1998).
[36] J. Theiler, S. Eubank, A. Longtin, B. Galdrikian, and J. D. Farmer, Physica D **58**, 77 (1992).
[37] The data set can be downloaded at http://www.fil.ion.ucl.ac.uk/spm/data/auditory
[38] A. M. Smith, B. K. Lewis, U. E. Ruttimann, F. Q. Ye, T. M. Sinnwell, Y. Yang, J. H. Duyn, and J. A. Frank, Neuroimage **9**, 526 (1999).
[39] W. H. Press, B. P. Flannery, S. A. Teukolsky, and W. T. Vetterling, *Numerical Recipes* (Cambridge University Press, Cambridge, UK, 1992).
[40] S. Kim, J. Ashe, K. Hendrich, J. M. Ellermann, H. Merkle, K. Ugurbil, and A. P. Georgopoulos, Science **261**, 615 (1993).
[41] J. R. Binder, S. M. Rao, T. A. Hammeke, Y. Z. Yetkin, A. Jesmanowicz, P. A. Bandettini, E. C. Wong, L. D. Estkowski, M. D. Goldstein, V. M. Haughton *et al.*, Ann. Neurol. **35**, 662 (1994).
[42] T. Schreiber, Int. J. Bifurcat. Chaos **5**, 349 (1995).
[43] C. Merkwirth, U. Parlitz, and W. Lauterborn, Phys. Rev. E **62**, 2089 (2000).
[44] B. R. Rosen, R. L. Buckner, and A. M. Dale, Proc. Natl. Acad. Sci. U.S.A. **95**, 773 (1998).
[45] T. W. Liao, Pattern Recognit. **38**, 1857 (2005).
[46] R. Heller, D. Stanley, D. Yekutieli, N. Rubin, and Y. Benjamini, Neuroimage **33**, 599 (2006).